doi:10.1006/jmbi.2000.3913 available online at http://www.idealibrary.com on IDEAL® *J. Mol. Biol.* (2000) **300**, 987–994

JMB

The Fold of Human Aquaporin 1

Bert L. de Groot[1], J. Bernard Heymann[2], Andreas Engel[2] Kaoru Mitsuoka[3], Yoshinori Fujiyoshi[3] and Helmut Grubmüller[1]*

[1]*Max Planck Institute for Biophysical Chemistry Theoretical Molecular Biophysics Group, Am Fassberg 11 D-37077, Göttingen Germany*

[2]*M.E. Müller Institute for Microscopic Structural Biology Biozentrum, University of Basel, CH-4056, Switzerland*

[3]*Department of Biophysics Faculty of Science, Kyoto University, Kitashirakawa Kyoto, 606-01, Japan*

**Corresponding author*

The fold of human aquaporin 1 is determined from cryo-electron microscopic data at 4.5 Å resolution. The monomeric structure consists of two transmembrane triple helices arranged around a pseudo-2-fold axis connected by a long flexible extracellular loop. Each triplet contains between its second and third helix a functional loop containing the highly conserved fingerprint NPA motif. These functional loops are assumed to fold inwards between the two triplets, thereby forming the heart of the water channel. The helix topology was determined from the directionality pattern of each of the six transmembrane helices with respect to the membrane, together with constraints defined by the sequence and atomic force microscopy data. The directionality of the helices was determined by collecting the best-fitting orientations resulting from a search through the three-dimensional experimental map for a large number of α-helical fragments. Tests on cryo-electron crystallographic bacteriorhodopsin data suggest that our method is generally applicable to determine the topology of helical proteins for which only medium-resolution electron microscopy data are available.

© 2000 Academic Press

Keywords: protein structure; electron microscopy; water transport; helix assignment; membrane protein

Introduction

Aquaporin 1 (AQP1) was the first specific water channel characterised (Preston *et al.*, 1992). Since then, many homologous water channels have been found in various organisms (Agre *et al.*, 1998; Heymann & Engel, 2000). Although many features of the water channel have been studied by numerous techniques, its remarkable efficiency and selectivity in transporting water are still poorly understood, and structural data will be invaluable in this respect. Earlier studies at lower resolution showed that AQP1 forms homotetramers *in vivo* (Verbavatz *et al.*, 1993) with each monomer containing six transmembrane helices (Walz *et al.*, 1997; Cheng *et al.*, 1997; Li *et al.*, 1997), in agreement with a hydropathy analysis based on the sequence (Preston & Agre, 1991) and with spectroscopic data (Cabiaux *et al.*, 1997). Since then, the resolution of structural studies on AQP1 has been steadily improved, and the most recent dataset obtained by cryo-electron microscopy was collected at 4.5 Å (Mitsuoka *et al.*, 1996b).

A prerequisite for any protein structure determination is knowledge of the correct fold (or helix packing arrangement for α-helical proteins). If only low-resolution data are available, as is the case for AQP1, this is a formidable challenge. For AQP1, there are 1440 ($=2 \times 6!$) possible helix packing topologies (Cheng *et al.*, 1997). The three-dimensional electron crystallographic potential map (the equivalent of an electron density map in X-ray crystallography) lacks strong side-chain features (Figure 1), which renders a straightforward assignment of the six pieces of (predicted) helical sequence to the six stretches of cylindrical density in the map, sketched in Figure 2, impossible. Moreover, the experimental map is diffuse in the loop regions, which complicates the tracing of the polypeptide chain from one helix to the next, a general problem in electron crystallography. However, a number of constraints from different sources restrict the huge number of possible folds, and thus renders identification of the correct fold tractable.

Abbreviations used: AQP1, aquaporin 1; BR, bacteriorhodopsin; EM, electron microscopy.

E-mail address of the corresponding author: hgrubmu@gwdg.de

0022-2836/00/040987–8 $35.00/0

© 2000 Academic Press

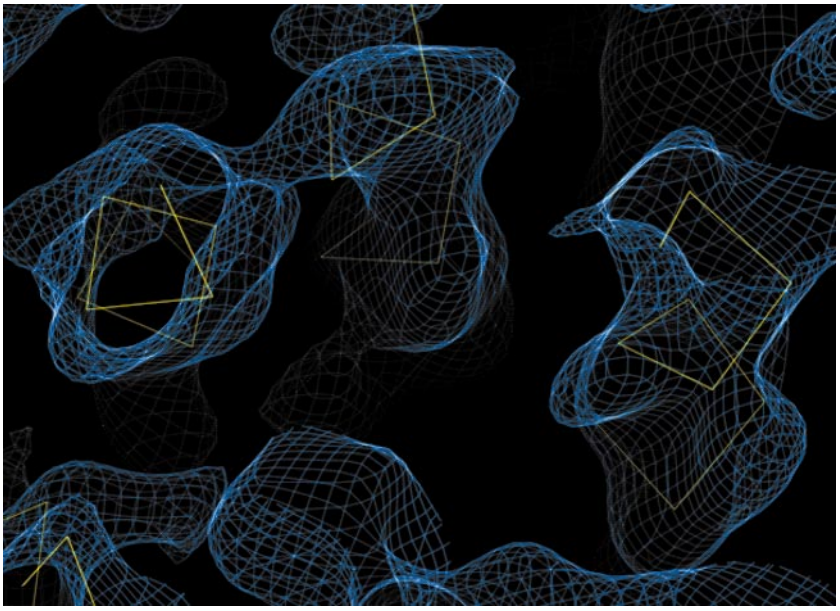

Figure 1. Detail of the electron-crystallographic potential map at 4.5 Å resolution. The map was contoured at 1.2 σ and modelled α-carbon traces of α-helices are superimposed (rendered using the program O (Jones *et al*., 1991)).

A first constraint on the topology is formed by the internal amino acid sequence similarity between the two halves of the molecule throughout the aquaporin family (Preston & Agre, 1991; Heymann & Engel, 2000). This quasi-symmetry has been suggested to correspond to a clear non-crystallographic pseudo-symmetry in the low-resolution structure (Li *et al*., 1997; Cheng *et al*., 1997). The consensus for the structure of the central part of the water channel is that the two highly conserved NPA motifs are located between the two triplets of helices that are believed to form the monomer, as suggested by the so-called hourglass model (Jung *et al*., 1994). From the 1440 possible models, only 96 show this internal structural symmetry (Cheng *et al*., 1997), and these remain to be considered.

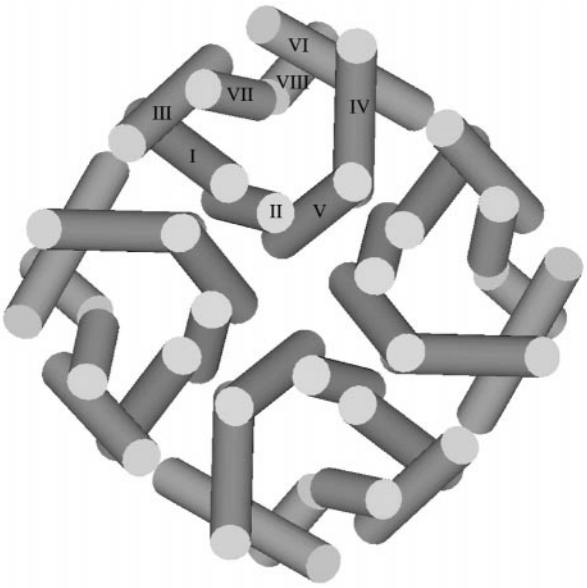

Figure 2. Arrangement of α-helices in the AQP1 tetramer (see (Heymann & Engel, 2000)). The six transmembrane helical electron densities of each of the monomers are numbered I through VI. The two short helices VII and VIII consist of the C-terminal halves of the functional B and E loops (Mitsuoka *et al*., 1999b).

A second restriction arises from the fact that the A loop between helices 1 and 2 and the D loop between helices 4 and 5 are relatively short throughout the aquaporin family (with a minimum of six and three residues, respectively (Heymann & Engel, 2000)). Thus, the C termini of helices 1 and 4 must be close to the N termini of helices 2 and 5, respectively. This constraint, together with the first one of internal structural symmetry, reduces the number of possible helix topologies to 16.

A third constraint is set by the sidedness of AQP1 crystals, which was determined by metal-shadowing and atomic force microscopy (Scheuring *et al*., 1999, 2000). This constraint restricts the number of possible helix topologies by another factor of two. The eight folds that fulfil all three constraints are shown in Figure 3.

The goal of this study is to unambiguously derive the correct AQP1 fold from the electron microscopy (EM) data among these eight helix topologies. Since the backbone of α-helices is right-handed both from N to C terminus and from C to N terminus, the only feature that can be exploited to distinguish the directionality of an α-helix in a density map is the asymmetry of the side-chains and the direction of the main-chain hydrogen bonds. It is a well-known feature of α-helices that, generally, the side-chains tend to point towards the N terminus. Therefore, model helices should fit better in the experimental map in one orientation than in the opposite, for each of stretch of helical

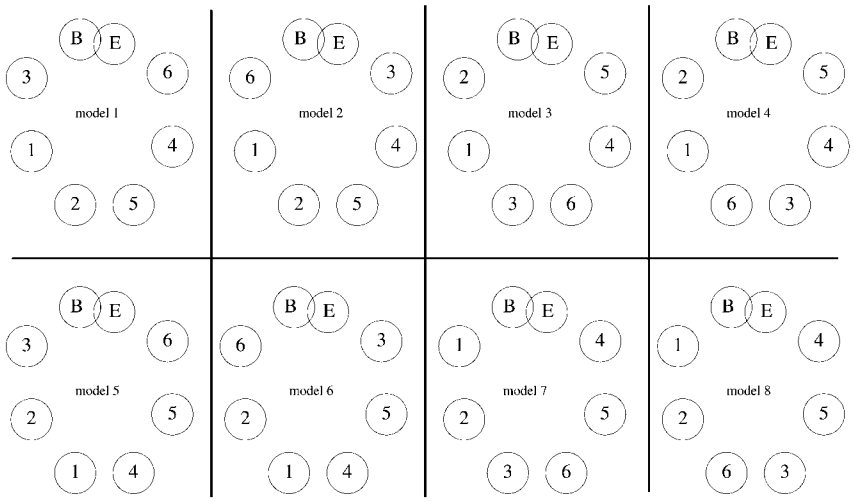

Figure 3. Only eight out of a total of 1440 possible folds (seen from the extracellular side) fulfil the constraints of internal pseudo-symmetry, short A and D loops, and overall sidedness. The circles correspond to the regions of α-helical density in the upper monomer in Figure 2. The numbers 1 through 6 denote the six transmembrane helices in the amino acid sequence of AQP1, as determined from hydropathy analyses, and B/E refers to the functional B and E loops, which together form a kinked helix.

density. In the spirit of programs such as essens (Kleywegt & Jones, 1997) and fffear (Cowtan, 1998), we have exhaustively searched the three-dimensional map for the most likely location of a large number of model α-helices. Such a systematic search, possible due to the availability of both amplitudes and phases in electron crystallography, should allow the directionality of each of the six transmembrane helices to be determined.

Combined with the other constraints on the topology, the determination of the orientation of each of the six helices should allow identification of the correct fold of AQP1.

Methods

A systematic real-space rigid body rotation and translation search of a large set of α-helical structural fragments (''probe helices'') was performed through the three-dimensional experimental map (Mitsuoka *et al.*, 1996b) to find their most probable locations. A software package was developed for this purpose (obtainable free from http://www.mpibpc.gwdg.de/abteilungen/071/bgroot/maptools.html) with added functionality with respect to existing programs such as essens from the Rave software package (Kleywegt & Jones, 1997) and fffear (Cowtan, 1998).

For a given structural fragment, the program rottrans performs a full rotation and translation search through a three-dimensional (experimental) map and outputs the scores for the best-fitting orientations. Steps of 1.0 Å and 10° (evenly distributed on a sphere) were taken for the translations and rotations, respectively. Scores are defined as the correlation coefficient between computed and experimental densities over a set of grid points in the vicinity of the probe helices. Only those grid points were considered which were closer than 2.5 Å to the nearest atom of the probe helix.

A set of 38 α-helical fragments was extracted from the Protein Data Bank and taken as probe helices for rottrans. We found that the use of a set of realistic probe helices gave better results than a single model α-helix. Helices with lengths varying between six and 13 amino acid residues were isolated from structures of bacteriorhodopsin (Grigorieff *et al.*, 1996), light-harvesting complex (Koepke *et al.*, 1996), photosynthetic reaction center (McAuley-Hecht *et al.*, 1998), haemoglobin (Fermi *et al.*, 1984), T4 lysozyme (Weaver & Matthews, 1987), the B domain of protein G (Gallagher *et al.*, 1994), potassium channel (Doyle *et al.*, 1998), cytochrome C′ (Dobbs *et al.*, 1996), apolipoprotein E2 (Dong *et al.*, 1996), ROP (Vlassi *et al.*, 1998). The obtained helical fragments were mutated to polyvaline by the WHAT IF program (Vriend, 1990).

For the calculated densities, a uniform isotropic *B*-factor of 50 Å^2 was applied. To amplify the asymmetry of the α-helices, valine was used instead of the more commonly used alanine.

Separate rottrans runs were performed for each of the probe helices, based on masks created for each of the six regions in the map where transmembrane α-helices were suspected, resulting in $6 \times 38 = 228$ calculations. Masks were defined as the collection of grid points in the experimental map with a distance of less than 2.5 Å from the principal axes of the corresponding helical region in the map. In the search, only those fragments were taken into account that had their centre of gravity within the mask and had a principal axis tilted by less than 20° with respect to the principal axis of the mask. The 100 best-fitting orientations from each run were collected equidistant along the principal helix axis. The preferred directionality for each of the six helices was subsequently derived from the number of fragments in both orientations and their average scores.

As a test case, the procedure as outlined above was carried out for the seven transmembrane helices of bacteriorhodopsin (BR), with cryo-electron microscopic data up to 3.5 Å (Henderson *et al.*, 1990) and up to 3.0 Å (Mitsuoka *et al.*, 1999a). The bias introduced by the presence of BR helices (Grigorieff *et al.*, 1996) in the set of the 38 probe

helices is negligible, since in each case the correct orientation is only one out of 3800 probed orientations.

Here, the six pieces of amino acid sequence that correspond to the six transmembrane helices of AQP1 are numbered 1 through 6 (1 through 7 for BR) and the stretches of α-helical density in the experimental potential map are numbered I through VI for the transmembrane helices, as defined in the legend to Figure 2. The functional loops in AQP1, that together form a highly kinked helix in the map, are denoted by VII and VIII. In BR, the seven transmembrane helical regions in the map are numbered I through VII (corresponding to the helical amino acid sequence pieces 1 through 7, respectively).

Results

Bacteriorhodopsin

In the structure of BR the seven transmembrane helices are arranged in a down-up-down-up-down-up-down pattern (with down defined as having the N terminus extracellular). Figure 4 shows the results of a series of rottrans runs on the 3.5 Å resolution dataset of BR (Henderson *et al.*, 1990). The plots show all fragments/orientations (sorted to score) with a correlation between experimental and calculated densities of more than 0.3, in both directionalities (continuous and broken lines). The orientations of the helices in regions I, II, III, V and VII turn out to be correctly predicted (i.e. the correct directionality is found more often and with a higher average score than the opposite directionality), whereas the results for regions IV and VI are not significant. For the data at 3.0 Å (Mitsuoka *et al.*, 1999a) (Figure 5), the orientation of the helices in regions IV and VI can also be identified, and therefore the correct directionality for each of the seven helices is obtained.

Aquaporin 1

Figure 6 shows the rottrans results for each of the AQP1 helices. At the positions of helices I, III, V and VI, more fragments are found with their N termini intracellular and the C termini extracellular (or up, broken lines), whereas helices II and IV show a preference for helices with their N termini extracellular and the C termini intracellular (or down, continuous lines).

Unfortunately, the obtained directionality pattern does not correspond to any of the models in Figure 3, because the obtained pattern violates the internal structural symmetry constraint. However, the directionality pattern is very close to that of models 1, 2 and 4 from Figure 3, with helix VI violating model 1 and helix III violating models 2 and 4. A closer inspection of the directionality analysis of helix VI shows that the apparently significant preference for the up orientation is in fact mislead-

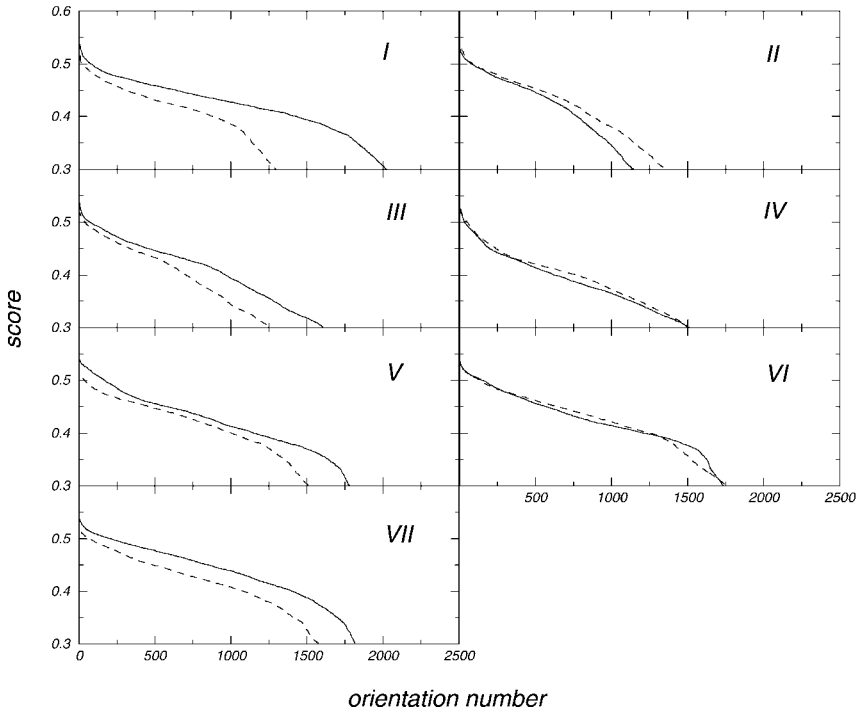

Figure 4. Scores from fragments fitted in the electron-crystallographic potential map of BR at 3.5 Å resolution (Henderson *et al.*, 1990). The panels numbered I through VII correspond to the seven transmembrane helical regions in the BR map. For each helical position, scores for model helical fragments in the down (continuous line) and up (broken line) orientations are depicted (with up defined as having the N terminus intracellular and the C terminus extracellular), sorted to score.

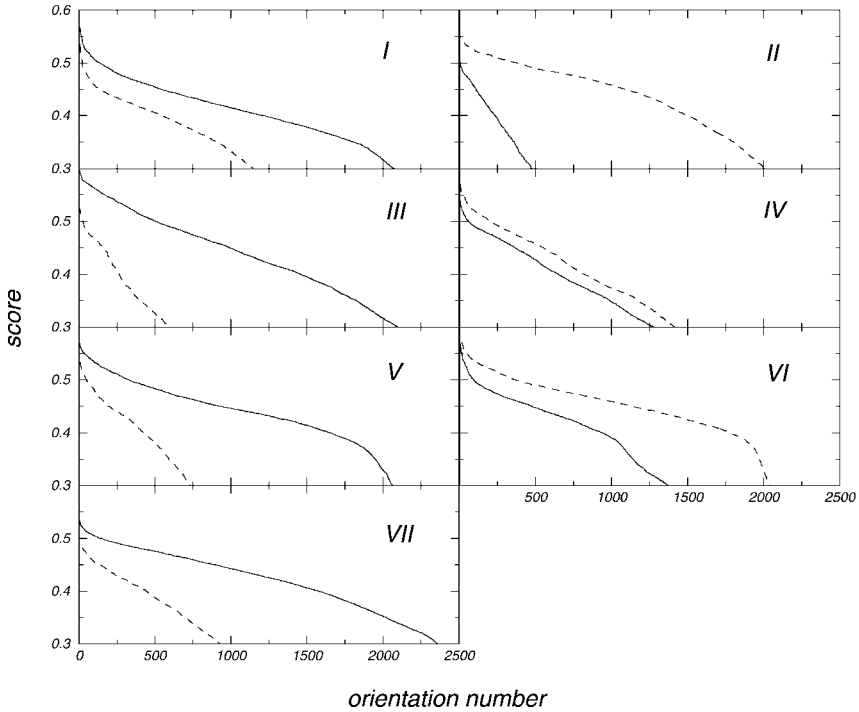

Figure 5. Scores from fragments fitted in the electron-crystallographic potential map of BR at 3.0 Å resolution (Mitsuoka *et al.*, 1999a). For notation, see the legend to Figure 4.

ing: as can be seen in Figure 7, the prefered up orientation is dominated by the upper half of the helix; the lower half shows a strong preference for the down orientation. Note that the other five regions show a consistent preference for one of the two orientations in both halves. The ambiguity of the directionality of the helix in region VI is further illustrated by a preference for the down orientation

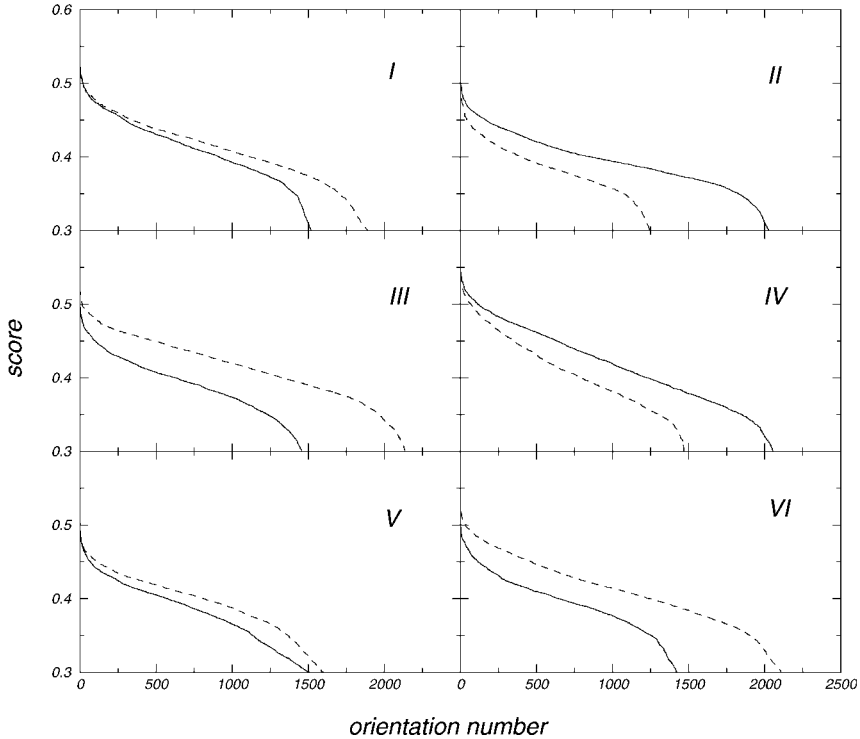

Figure 6. Scores from fragments fitted in the electron-crystallographic potential map of AQP1. The panels numbered I through VI correspond to the six stretches of α-helical density in the experimental map, as defined in the legend to Figure 2. For details, see Figure 4.

for the upper half of region VI in an analysis with poly-alanine probe helices (data not shown). In region III, however, probe helices on average score better in the up orientation throughout the whole region (Figure 7). This indicates that region VI, rather than helix III, contains a helix in the down orientation.

Taken together, these results strongly suggest model 1 depicted in Figure 3 as the correct fold of AQP1. Figure 8 schematically shows the AQP1 structure with the six transmembrane helices and connecting loops.

Discussion

The determination of the directionality of α-helices based on electron-crystallographic data at a lower resolution than 3 Å is non-trivial, as illustrated by the BR (Figure 4) and AQP1 results (Figures 6 and 7). We found that the use of poly-valine probe helices yields more reliable results than poly-alanine helices. This can be rationalised because, as stated above, the structural asymmetry of α-helices is caused mainly by the side-chains and, therefore, poly-valine probe helices give rise to a stronger signal than poly-alanine helices. The disadvantage of using poly-valine probe helices, however, is that additional noise enters the analyses due to errors in the chosen side-chain rotamer states and due to the fitting of too many side-chain atoms at Gly and Ala positions. This is the most probable explanation for the problematic determination of the directionality of the helix in region VI in the map of AQP1: the upper half of this helix possibly has a number of unusual side-chain conformations that cause the poly-valine results to be unreliable (Figure 7). This assumption is supported by the fact that also for BR, the two helical regions for which it is most difficult to determine the directionality, regions IV and VI (Figure 4), are also the most unusual in their amino acid composition and their side-chain conformations: helix 4 contains an alanine or glycine residue in nine out of 20 positions in the membrane region, and helix 6 contains two tryptophan residues and a tyrosine residue, which interact directly with the retinal, and have unusual rotamer states. In AQP1, the N-terminal half of helix 6 contains two tryptophan residues and a phenylalanine residue, which could explain the ambiguity for region VI in the AQP1 map.

For the three datasets we studied, a comparison of rottrans to essens from the rave software package (Kleywegt & Jones, 1997) and to fffear (Cowtan, 1998) shows that the use of a mask to preselect not only translations but also rotations for the probe helices makes our implementation extremely efficient (using the parameters as mentioned in Methods, one run takes less than a

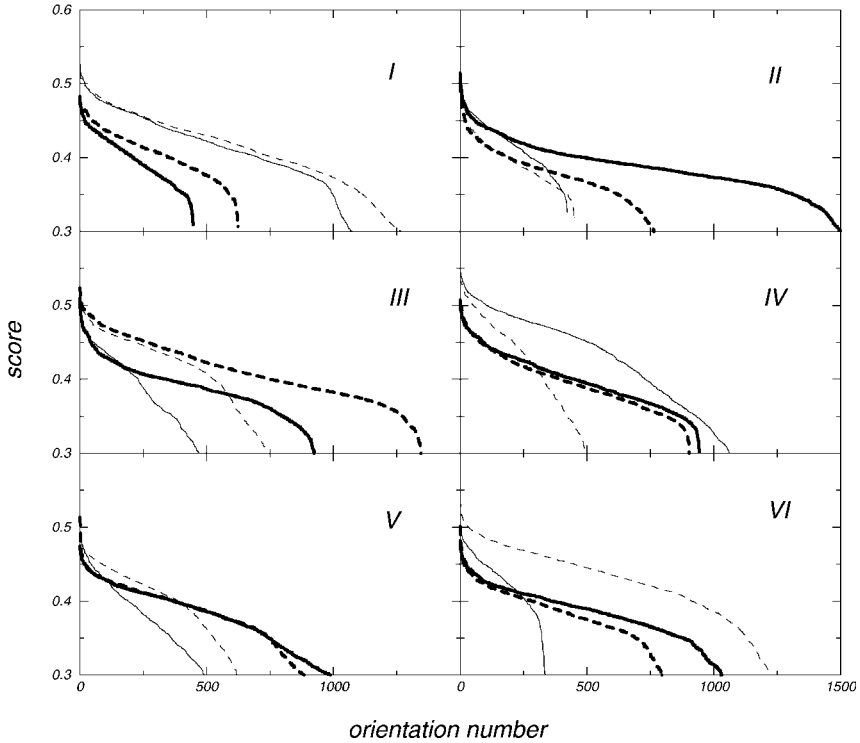

Figure 7. Scores from fragments fitted in the electron-crystallographic potential map of AQP1. The panels numbered I through VI correspond to the six stretches of α-helical density in the experimental map, as defined in the legend to Figure 2. The thin curves refer to the upper half (along the helical axis) and the bold curves to the lower half of each of the helical regions, respectively. As in Figures 4, 5 and 6, scores for model helical fragments in the down orientation are depicted by continuous lines and those in the up orientation by broken lines.

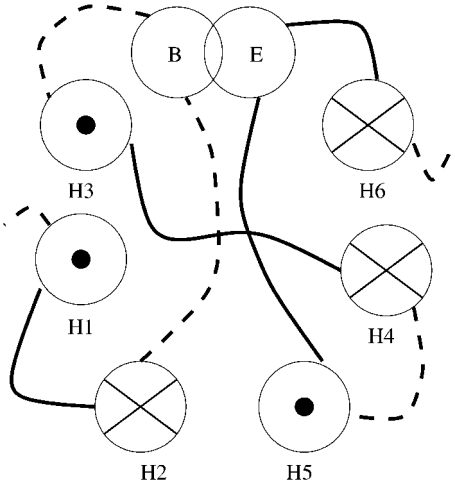

Figure 8. Proposed AQP1 fold, looking at the monomer from the extracellular side. The orientation of each of the helices is indicated by ⊙ for up and ⊗ for down. Intracellular and extracellular loops are sketched by broken and continuous lines, respectively. This model corresponds to model 1 in Figure 3.

minute on a typical workstation). The correlation scoring function applied here is possibly inferior to a least-squares or maximum-likelihood scoring function. However, it has the advantage that it is scale invariant and therefore does not require an estimate of the absolute scale of the experimental densities. It is therefore the method of choice when such an estimate is difficult or undesirable, as is the case for the medium-resolution datasets we studied. We found that the method of collecting fragments as implemented in our software (the best-scoring fragments spaced equidistant along the principal helix axis) yields better results than simply collecting the best-scoring fragments, since it reduces the risk that one part of the mask dominates others.

A striking feature of the obtained AQP1 fold is the location of the C loop, connecting the C terminus of helix 3 to the N terminus of helix 4. It would have to span the whole monomer on the extracellular side, thereby crossing the E loop. This implies a complicated folding pathway, supported by the minimal length of 16 residues that is observed in the sequences of the aquaporin family (Heymann & Engel, 2000), some weak density on the extracellular face of the molecule (Mitsuoka *et al.*, 1999b) and the elongated peripheral protrusion at the extracellular surface of AqpZ (Scheuring *et al.*, 1999). However, it is also conceivable that the C loop would connect to what is assumed to be the neighbouring monomer in the tetramer. Although we strongly prefer the original definition of the monomer, this alternative cannot be excluded at this stage, and studies at higher resolution are required to resolve this issue.

Conclusions

The fold of AQP1 has been determined from the 4.5 Å resolution three-dimensional electron-crystallographic map. Considerations derived from the sequence (internal symmetry, short A and D loops) and atomic force microscopy measurements had reduced the number of possible helix arrangements from 1440 to eight, but the lack of strong side-chain features and the diffuse loop regions in the experimental density map made it difficult to assign the helices in the experimental density map. An enhanced method to search for the most probable locations of probe helices in the experimental map, however, allowed the determination of the directionality of each of the six transmembrane helices. This in turn facilitated the identification of one helix topology as best candidate among the remaining eight folds.

The obtained fold is in perfect agreement with a detailed sequence analysis of the aquaporins (Heymann & Engel, 2000) which predicted that helices 2 and 5 would occupy the inner helices of the tetramer, and helices 3 and 6 correspond to the outer, long tilted helices facing the functional B and E loops, leaving helices 1 and 4 for the intermediate helices. Also the analysis of correlated mutations presented there corresponds well to this model.

A general, systematic and efficient method has been developed and tested to determine a protein's fold on the basis of medium-resolution (~4 Å) data. The correct identification of our test case, BR, as well as the consistent identification of the AQP1 fold, strongly suggest that this technique will have broad applicability in the rapidly expanding field of medium-resolution crystallography.

Acknowledgements

We thank Gerard Kleywegt for useful suggestions on using the essens program, Kevin Cowtan for his help on the fffear program and Dimitri Fotiadis and Simon Scheuring for stimulating discussions. BdG was supported by the BIOTECH program of the EU, grant nr. BIO4-CT98-0024. KM and YF were supported by the Japan Society for the Promotion of Science (JSPS-RFTF96L00502).

References

Agre, P., Bonhivers, M. & Borgnia, M. J. (1998). The aquaporins, blueprints for cellular plumbing systems. *J. Biol. Chem.* **273**, 14659-14662.

Cabiaux, V., Oberg, K. A., Pancoska, P., Walz, T., Agre, P. & Engel, A. (1997). Secondary structures comparison of aquaporin-1 and bacteriorhodopsin: a fourier transform infrared spectroscopy study of two-dimensional membrane crystals. *Biophys. J.* **73**, 406-417.

Cheng, A. C., Van Hoek, A. N., Yeager, M., Verkman, A. S. & Mitra, A. K. (1997). Three-dimensional

organization of a human water channel. *Nature,* **387**, 627-630.

Cowtan, K. (1998). Modified phased translation functions and their application to molecular fragment location. *Acta Crystallog. sect. D,* **54**, 750-756.

Dobbs, A. J., Anderson, B. F., Faber, H. R. & Baker, E. N. (1996). Three-dimensional structure of cytochrome C′ from two *Alcaligenes* species and the implications for four-helix bundle structures. *Acta Crystallog. sect. D,* **52**, 356-368.

Dong, L. M., Parkin, S., Trakhanov, S. D., Rupp, B., Simmons, T., Arnold, K. S., Newhouse, Y. M., Innerarity, T. L. & Weisgraber, K. H. (1996). Novel mechanism for defective receptor binding of apolipoprotein E2 in type III hyperlipoproteinemia. *Nature Struct. Biol.* **3**, 718-722.

Doyle, D. A., Cabral, J. M., Pfuetzner, R. A., Kuo, A. L., Gulbis, J. M., Cohen, S. L., Chait, B. T. & MacKinnon, R. (1998). The structure of the potassium channel: molecular basis of K^+ conduction and selectivity. *Science,* **280**, 69-77.

Fermi, G., Perutz, M. F., Shaanan, B. & Fourme, R. (1984). The crystal-structure of human deoxyhemoglobin at 1.74 Å resolution. *J. Mol. Biol.* **175**, 159-174.

Gallagher, T., Alexander, P., Bryan, P. & Gilliland, G. L. (1994). Two crystal structures of the B1 immunoglobulin-binding domain of streptococcal protein G and comparison with NMR. *Biochemistry,* **33**, 4721-4729.

Grigorieff, N., Ceska, T. A., Baldwin, J. M., Downing, K. H. & Henderson, R. (1996). Electron-crystallographic refinement of the structure of bacteriorhodopsin. *J. Mol. Biol.* **259**, 393-421.

Henderson, R., Baldwin, J., Ceska, T., Zemlin, F., Beckmann, E. & Downing, K. (1990). Model for the structure of bacteriorhodopsin based on high-resolution electron cryomicroscopy. *J. Mol. Biol.* **213**, 899-929.

Heymann, J. B. & Engel, A. (2000). Structural clues in the sequences of the aquaporins. *J. Mol. Biol.* **295**, 1039-1053.

Jones, T. A., Zou, J.-Y., Cowan, S. W. & Kjeldgaard, M. (1991). Improved methods for building protein models in electron density maps and the location of errors in these models. *Acta Crystallog. sect. A,* **47**, 110-119.

Jung, J. S., Preston, G. M., Smith, B. L., Guggino, W. B. & Agre, P. (1994). Molecular structure of the water channel through aquaporin CHIP - the hourglass model. *J. Biol. Chem.* **269**, 14648-14654.

Kleywegt, G. J. & Jones, T. A. (1997). Template convolution to enhance or detect structural features in macromolecular electron-density maps. *Acta Crystallog. sect. D,* **53**, 179-185.

Koepke, J., Hu, X. C., Muenke, C., Schulten, K. & Michel, H. (1996). The crystal structure of the light-harvesting complex II (B800-850) from *Rhodospirillum molischianum. Structure,* **4**, 581-597.

Li, H. L., Lee, S. & Jap, B. K. (1997). Molecular design of aquaporin-1 water channel as revealed by electron crystallography. *Nature Struct. Biol.* **4**, 263-265.

McAuley-Hecht, K. E., Fyfe, P. K., Ridge, J. P., Prince, S. M., Hunter, C. N., Isaacs, N. W., Cogdell, R. J. & Jones, M. R. (1998). Structural studies of wild-type and mutant reaction centers from an antenna-deficient strain of *Rhodobacter sphaeroides*: monitoring the optical properties of the complex from bacterial cell to crystal. *Biochemistry,* **37**, 4740-4750.

Mitsuoka, K., Hirai, T., Murata, K., Miyazawa, A., Kidera, A., Kimura, Y. & Fujiyoshi, Y. (1999a). The structure of bacteriorhodopsin at 3.0 Å resolution based on electron crystallography: implication of the charge distribution. *J. Mol. Biol.* **286**, 861-882.

Mitsuoka, K., Murata, K., Walz, T., Hirai, T., Agre, P., Heymann, J. B., Engel, A. & Fujiyoshi, Y. (1999b). The structure of aquaporin-1 at 4.5 Å resolution reveals short α-helices in the center of the monomer. *J. Struct. Biol.* **128**, 34-43.

Preston, G. M. & Agre, P. (1991). Isolation of the CDNA for erythrocyte integral membrane-protein of 28-kilodaltons - member of an ancient channel family. *Proc. Natl Acad. Sci. USA,* **88**, 11110-11114.

Preston, G. M., Carroll, T. P., Guggino, W. B. & Agre, P. (1992). Appearance of water channels in *Xenopus* oocytes expressing red-cell CHIP28 protein. *Science,* **256**, 385-387.

Scheuring, S., Ringler, P., Borgnia, M., Stahlberg, H., Müller, D., Agre, P. & Engel, A. (1999). High resolution AFM topographs of the *Escherichia coli* water channel aquaporin Z. *EMBO J.* **18**, 4981-4987.

Scheuring, S., Tittmann, P., Stahlberg, H., Ringler, P., Borgnia, M., Agre, P., Gross, H. & Engel, A. (2000). The aquaporins sidedness revisited. *J. Mol. Biol.* **299**, 1271-1278.

Verbavatz, J. M., Brown, D., Sabolic, I., Valenti, G., Siello, D. A., Van Hoek, A. N., Ma, T. & Verkman, A. S. (1993). Tetrameric assembly of CHIP28 water channels in liposomes and cell-membranes - a freeze-fracture study. *J. Cell Biol.* **123**, 605-618.

Vlassi, M., Dauter, Z., Wilson, K. S. & Kokkinidis, M. (1998). Structural parameters for proteins derived from the atomic resolution (1.09 Å) structure of a designed variant of the ColE1 ROP protein. *Acta Crystallog. sect. D,* **54**, 1245-1260.

Vriend, G. (1990). WHAT IF: a molecular modeling and drug design program. *J. Mol. Graph.* **8**, 52-56.

Walz, T., Hirai, T., Murata, K., Heymann, J. B., Mitsuoka, K., Fujiyoshi, Y., Smith, B. L., Agre, P. & Engel, A. (1997). The three-dimensional structure of aquaporin-1. *Nature,* **387**, 824-827.

Weaver, L. H. & Matthews, B. W. (1987). Structure of bacteriophage T4 lysozyme refined at 1.7 Å resolution. *J. Mol. Biol.* **193**, 189-199.

Edited by R. Huber

(Received 15 March 2000; received in revised form 1 June 2000; accepted 1 June 2000)